Journal of the Brazilian Society of Mechanical Sciences and Engineering (2024) 46:206
https://doi.org/10.1007/s40430-024-04818-w

TECHNICAL PAPER

Numerical model for calculation of hydraulic transients with two-phase flow and fluid–structure interaction

Pedro Henrique do Nascimento Rocha[1] · Josie Aguila Alves de Campos[1] · Micelli Rodrigues Camargo[1] · Marcelo da Silva Rocha[1]

Received: 19 June 2023 / Accepted: 23 February 2024 / Published online: 12 March 2024

Abstract

Fluid transport systems such as pipelines are subject to loads whenever changes in fluid momentum or in pipeline structure occur. These loads can generate extremely harmful hydraulic transients which may be responsible for several major accidents. This paper presents a model for the solution of these hydraulic transients, considering two-phase flow and fluid–structure interaction. Mathematical and numerical solutions are proposed and analyzed for the proper capture of the physical phenomena associated with the fluid compressibility and fluid celerity, which are variable in two-phase fluid, together with the disturbances generated by the fluid–structure interaction. The proposed solution for the model considers the simultaneous action of these phenomena. The developed numerical model is based on the solution of the mathematical model formed by a system of four partial differential equations, in which the necessary adaptations are integrated in fluid–structural equations and in the nonlinear mathematical coefficients for the solution of the compressible and two-phase flow in question. Classical formulation is selected for the implementation of friction between fluid and pipe in the model. For the solution, it is applied the method of characteristics and finite difference, with subsequent numerical integration. The validation of the results is carried out based on comparisons with experimental and analytical data. The model presented, in general, was quite adherent to the experimental and analytical results, mainly in relation to the first pressure peak, which is one of the main focuses of the transient analyses.

Keywords Hydraulic transients · Fluid–structure interaction · Method of characteristics · Two-phase gas–liquid flow · Numerical model

List of symbols

A	Previous point, pipe transversal area
f	Darcy–Weisbach friction coefficient
t	Time
V	Average fluid speed [m/s]
$\forall$	Volume
P	Average pressure [Pa]
L	Pipe length [m]
c	Celerity
Δ	Variation of a given entity
ρ	Density [kg/m^3]
g	Gravity acceleration [m/s^2]
K_{ut}	Time adjustment coefficient
K_{ux}	Length adjustment coefficient
R	Pipe internal radius
D	Pipe internal diameter [m]
e	Pipe thickness [m]
E	Pipe Young modulus (elasticity modulus)
ν	Poisson coefficient
p	Absolute pressure
K	Bulk modulus
γ	Pipe angle
τ_0	Friction term
i,cur	Counters
j	Time counter
α	Void fraction
K_v	Valve pressure loss coefficient
Cd	Outlet valve coefficient
m	Cd Adjustment coefficient
val	Valve
u, U	Pipe displacement
σ	Axial stress

Technical Editor: Erick Franklin.

✉ Pedro Henrique do Nascimento Rocha
pedrohenriquenrocha@usp.br

[1] Instituto de Pesquisas Energéticas e Nucleares—IPEN, University of São Paulo (USP), São Paulo, Brazil

N	Number of pipe sub-elements
λ	Wavelength

Coordinates and derivatives

z	Axial coordinate
t	Time coordinate
$\frac{\mathrm{d}}{\mathrm{d}t}$	Time total derivative
$\frac{\partial}{\partial t}$	Partial derivative in relation to t coordinate
$\frac{\partial}{\partial z}$	Partial derivative in relation to z coordinate

Subscripts

1,2,3,4	Characteristics curves
o	Reference to beginning
F,f	Fluid
t	*Pipe*
g	Gaseous phase
l	Liquid phase
out	External
max	Maximum
min	Minimum
rel	Relative
c	Valve closure
d,D	At right
e	At left
(i,j)	Position and time indicators in computational mesh
cur, i	Counter
cond	Condition
points	Number of points
z	Axial direction
m	Mixture

Superior and general points, marks and lines

~	Adjusted value
.	First derivative in time
-	Average value at transversal section
|	Taken at

Abbreviations

IAB	Instantaneous acceleration based
FSI	Fluid–structure interaction
MOC	Method of characteristics

1 Introduction

Fluid transport systems such as pipelines are subject to loads whenever changes in fluid momentum or in pipeline structure occur, either due to planned action, such as starting and stopping pumps and closing valves, or accidental such as, for example, rupture in pipes, sudden interruption of the flow, earthquakes, etc. These loads can generate extremely harmful hydraulic transients and may be responsible for several major accidents such as the accident occurred in the hydroelectric facility [1], and as demonstrated in the research pointed out by the study of the Electric Power Research Institute [2], in which 283 hydraulic transients in nuclear plants in the US between the years 1969 and 1988 were verified. Therefore, when the safety of the system in question is very critical, as in hydroelectric, thermonuclear, conventional thermoelectric, large transport of oil or big water supply networks, the hydraulic transients and their effects need to be very well known.

Besides, for the study of hydraulic transients to be more comprehensive and complete, in many cases, it is necessary to take into account important interactions that occur between the fluid and the piping structure during the transient. These interactions are commonly referred to as fluid–structure interaction (FSI), and they occur in all fluid transport pipelines. Furthermore, with regard more specifically to the type of flow, there are many practical cases of flow that occurs in the presence of two-phase fluid. Some examples of this type of flow can occur in systems, such as when the vapor phase appears in a situation of pressure drop during an accident with pipe rupture, when there is release of non-condensable gases or even during a steam generation process. Thus, as all these conditions can lead to a two-phase flow in pipes, the study of the behavior of two-phase fluid during a hydraulic transient together with FSI can be very important.

The recent work [3] presented a solution to simulate hydraulic transients in a typical system similar to the one studied in this paper: reservoir, pipe and valve; but considering the convective terms of the balance equations which are normally suppressed for one-phase flow, as demonstrated by Tijsseling [4]. With such consideration, it became possible to improve the simulation capability for cases where the pressure wave celerity can variate and become closer to the flow speed, as it can occur in two-phase flow in a system subjected to hydraulic transients. However, the model presented did not consider the FSI. The work developed by de Almeida [5] who proposed a solution with MOC for hydraulic transients also in the typical system, with FSI, but only applicable for one-phase flow. It is possible to notice that it was missing a formulation able of including both the wave celerity variation and also the FSI, using the MOC for solving the hydraulic transient. Thus, this paper aims at presenting a formulation also suppressing the convective terms, but still proposing a solution to include the celerities variation which take place for a two-phase flow and also including the capability of simulating the FSI with the piping system.

Finally, it can be summarized that the main objective of this paper is to present a one-dimensional numerical model capable of evaluating pressure and flow oscillations in a system where two-phase gas–liquid flow occurs with low void fraction and uniformly distributed bubbles, considering FSI,

making it possible to obtain the variables of interest for the type of system shown in Fig. 1, for homogeneous two-phase flow.

2 Mathematical method

The mathematical modeling was developed considering the models proposed by Ref. [5–8]. It is valid for straight, slender, circular section pipes with an axial degree of freedom. The pipes are externally in contact with a non-viscous fluid of constant pressure, so that they are not restricted in their movement. The pipe wall material is homogeneous, isotropic, linearly elastic and subject to small deformations. Resistance to inertial radial motion, bending stiffness and shear strain are ignored. Structural and fluid damping mechanisms are neglected, except for friction between the fluid and the pipe wall. The model is one-dimensional, with a spatial coordinate along the central axis of the pipe. This approach is valid for long wavelengths or low frequencies (long wavelength approximation, $\lambda \gg D$). Thin-walled pipes (D/e ratio > 25) are considered.

For the two-phase fluid, a homogeneous mixture with low void fractions and dispersed bubbles is considered according to the flow classification defined by Fernandes [9]; and according to the proposed model and experiment presented by Chaudry [8]. For fluid density and compressibility, a definition of homogeneous mixture applicable to two-phase fluid with low void fraction and negligible slip between phases is considered. In this way, the contained fluid is considered as Newtonian with homogeneous, isotropic and linearly elastic properties. Isothermal conditions prevail, considering the liquid phase as a great heat sink. The pressure inside the bubble is independent of surface tension and vapor pressure.

As assumed for flows of single-phase liquid with very low Mach numbers (relationship between flow velocity and wave propagation velocity in the flow), the convective acceleration terms are also neglected [5, 6]. Although the propagation velocity in the medium can be considerably lower for a gas–liquid mixture than for the single-phase liquid itself, causing the fluid velocity to be reduced substantially to attenuated values [10, 11], the proposed model will focus on cases with the Mach number still quite low, due to the relatively small flow velocities (in the simulated case presented further, V_o represents 2.6% of the smaller fluid celerity occurred during the transient), according to the fluid equations presented in Ref. [8]. Therefore, the fluid (V) and pipe ($\dot{u}_z$) velocities are considered much smaller than the wave velocities in the two-phase fluid (c_F) and in the pipe (c_t).

As demonstrated by Tijsseling [6], the four equations that describe the behavior of the fluid and the structure during the transient are presented below:

Fluid:

$$\frac{\partial V}{\partial t} + \frac{1}{\rho_f}\frac{\partial P}{\partial z} = -\frac{2}{\rho_f R}\tau_0 + g\sin\gamma \tag{1}$$

$$\frac{\partial V}{\partial z} + \frac{1}{\rho_f c_F^2}\frac{\partial P}{\partial t} = 2\nu\frac{\partial \dot{u}_z}{\partial z} \tag{2}$$

Pipe:

$$\frac{\partial \dot{u}_z}{\partial t} - \frac{1}{\rho_t}\frac{\partial \sigma_z}{\partial z} = \frac{\rho_f A_f}{\rho_t A_t}\frac{2}{\rho_f R}\tau_0 + g\sin\gamma \tag{3}$$

$$\frac{\partial \dot{u}_z}{\partial z} - \frac{1}{\rho_t c_t^2}\frac{\partial \sigma_z}{\partial t} = -\frac{\nu R}{Ee}\frac{\partial P}{\partial t} \tag{4}$$

where classical celerities are defined as follows:

$$c_F^2 = \left[\rho_f\left(\frac{1}{K} + \left(1-\nu^2\right)\frac{2R}{Ee}\right)\right]^{-1} \tag{5}$$

$$c_t^2 = \frac{E}{\rho_t} \tag{6}$$

Equations (5) and (6) correspond to the celerities, respectively, associated to the propagation speeds of the pressure waves in the fluid and of the stress waves in the pipe.

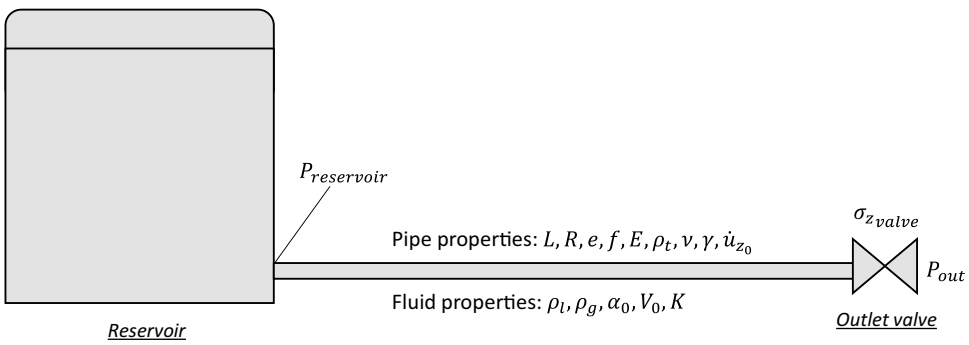

Fig. 1 System drawing. *Source*: Author

2.1 Properties of the two-phase fluid

It is considered that a gas–liquid mixture has variable bulk modulus K and density ρ_f. Based on [7], Eqs. (7) and (8) that describe ρ_f and K variables are presented, together with Eq. (9) for variable α (considering that bubbles behave isothermally during the transient).

$$\rho_f = \rho_l(1-\alpha) + \alpha\rho_g \tag{7}$$

$$K = \frac{1}{\frac{\alpha}{p} + \frac{1}{K_l}} \tag{8}$$

$$\alpha p = \alpha_0 p_0 \tag{9}$$

$$\alpha = \frac{\forall_g}{\forall_m} \tag{10}$$

2.2 Steady friction

Considering the static friction model, the shear stress term τ_o is assumed to be the same as that of a stable flow. In terms of the Darcy–Weisbach friction factor, the friction τ_o indicated in the balance Eqs. (1) and (3) is composed of the static friction τ_s, defined as follows:

$$\tau_0 = \tau_s = \rho_f f \frac{V_{\text{rel}}\left|V_{\text{rel}}\right|}{8} \tag{11}$$

where V_{rel} is the one-dimensional relative velocity $V - \overline{\dot{u}_z}$ between the liquid and the pipe wall, and f is the Moody friction factor, considered as constant.

2.3 Method of characteristics (MOC)

The method of characteristics (MOC) is a mathematical solution method for hyperbolic systems of partial differential equations, based on Riemann invariants, in which characteristic curves are established in the domain (z,t), so that on these curves, the system's equations can be rewritten as total derivatives with respect to the variable of interest (in this case t). When applying the MOC to Eqs. (1)–(4), the aim is to establish the curves in the domain in which this system can be rewritten as a system of total differential equations, which are then called as characteristic equations. The characteristic equations produced are presented below, defined according to the method proposed by [6], assuming the hypotheses previously described at the beginning of Sect. 2:

$$\begin{aligned}
&\left(\frac{\mathrm{d}V}{\mathrm{d}t}\right)_1 + \frac{1}{c_F|_1}\left[\frac{1}{\rho_f|_1}\left(\frac{\tilde{c}_F|_1}{c_F|_1}\right) + 2\nu^2\frac{R}{e}\frac{1}{\rho_t}\frac{\frac{(c_F|_1\,\tilde{c}_F|_1)}{c_t^2}}{1-\left(\frac{\tilde{c}_F|_1}{c_t}\right)^2}\right]\left(\frac{\mathrm{d}P}{\mathrm{d}t}\right)_1 \\
&+ 2\nu\frac{\left(\frac{\tilde{c}_F|_1}{c_t}\right)^2}{1-\left(\frac{\tilde{c}_F|_1}{c_t}\right)^2}\left(\frac{\mathrm{d}\dot{u}_z}{\mathrm{d}t}\right)_1 - \frac{2\nu}{\rho_t\,\tilde{c}_F|_1}\frac{\left(\frac{\tilde{c}_F|_1}{c_t}\right)^2}{1-\left(\frac{\tilde{c}_F|_1}{c_t}\right)^2}\left(\frac{\mathrm{d}\sigma_z}{\mathrm{d}t}\right)_1 \\
&= -\frac{2}{\rho_f|_1 R}\tau_0 + g\sin\gamma + 2\nu\frac{\left(\frac{\tilde{c}_F|_1}{c_t}\right)^2}{1-\left(\frac{\tilde{c}_F|_1}{c_t}\right)^2}\left(\frac{\rho_f|_1 A_f}{\rho_t A_t}\frac{2}{\rho_f|_1 R}\tau_0 + g\sin\gamma\right)
\end{aligned} \tag{12}$$

$$\text{on the line}: \frac{\mathrm{d}z}{\mathrm{d}t} = \tilde{c}_F|_1 \tag{13}$$

$$\begin{aligned}
&\left(\frac{\mathrm{d}V}{\mathrm{d}t}\right)_2 \\
&- \frac{1}{c_F|_2}\left[\frac{1}{\rho_f|_2}\left(\frac{\tilde{c}_F|_2}{c_F|_2}\right) + 2\nu^2\frac{R}{e}\frac{1}{\rho_t}\frac{\frac{(c_F|_2\,\tilde{c}_F|_2)}{c_t^2}}{1-\left(\frac{\tilde{c}_F|_2}{c_t}\right)^2}\right]\left(\frac{\mathrm{d}P}{\mathrm{d}t}\right)_2 \\
&+ 2\nu\frac{\left(\frac{\tilde{c}_F|_2}{c_t}\right)^2}{1-\left(\frac{\tilde{c}_F|_2}{c_t}\right)^2}\left(\frac{\mathrm{d}\dot{u}_z}{\mathrm{d}t}\right)_2 + \frac{2\nu}{\rho_t\,\tilde{c}_F|_2}\frac{\left(\frac{\tilde{c}_F|_2}{c_t}\right)^2}{1-\left(\frac{\tilde{c}_F|_2}{c_t}\right)^2}\left(\frac{\mathrm{d}\sigma_z}{\mathrm{d}t}\right)_2 \\
&= -\frac{2}{\rho_f|_2 R}\tau_0 + g\sin\gamma + 2\nu\frac{\left(\frac{\tilde{c}_F|_2}{c_t}\right)^2}{1-\left(\frac{\tilde{c}_F|_2}{c_t}\right)^2}\left(\frac{\rho_f|_2 A_f}{\rho_t A_t}\frac{2}{\rho_f|_2 R}\tau_0 + g\sin\gamma\right)
\end{aligned} \tag{14}$$

$$\text{on the line}: \frac{\mathrm{d}z}{\mathrm{d}t} = -\tilde{c}_F|_2 \tag{15}$$

$$\begin{aligned}
&-\nu\frac{R}{e}\frac{\rho_f|_3}{\rho_t}\frac{\left(\frac{c_F|_3}{c_t}\right)^2}{1-\left(\frac{c_F|_3}{\tilde{c}_t|_3}\right)^2}\left(\frac{\mathrm{d}V}{\mathrm{d}t}\right)_3 \\
&-\nu\frac{R}{e}\frac{1}{\rho_t}\frac{1}{c_t}\frac{\tilde{c}_t|_3}{c_t}\frac{\left(\frac{c_F|_3}{\tilde{c}_t|_3}\right)^2}{1-\left(\frac{c_F|_3}{\tilde{c}_t|_3}\right)^2}\left(\frac{\mathrm{d}P}{\mathrm{d}t}\right)_3 \\
&+\left[1+2\nu^2\frac{R}{e}\frac{\rho_f|_3}{\rho_t}\frac{\left(\frac{c_F|_3}{c_t}\right)^2}{1-\left(\frac{c_F|_3}{\tilde{c}_t|_3}\right)^2}\right]\left(\frac{\mathrm{d}\dot{u}_z}{\mathrm{d}t}\right)_3 \\
&-\frac{1}{\rho_t c_t}\frac{\tilde{c}_t|_3}{c_t}\left(\frac{\mathrm{d}\sigma_z}{\mathrm{d}t}\right)_3 = \left[1+2\nu^2\frac{R}{e}\frac{\rho_f|_3}{\rho_t}\frac{\left(\frac{c_F|_3}{c_t}\right)^2}{1-\left(\frac{c_F|_3}{\tilde{c}_t|_3}\right)^2}\right]\left(\frac{\rho_f|_3 A_f}{\rho_t A_t}\frac{2}{\rho_f|_3 R}\tau_0 + g\sin\gamma\right) \\
&+\nu\frac{R}{e}\frac{\rho_f|_3}{\rho_t}\frac{\left(\frac{c_F|_3}{c_t}\right)^2}{1-\left(\frac{c_F|_3}{\tilde{c}_t|_3}\right)^2}\left(\frac{2}{\rho_f|_3 R}\tau_0 + g\sin\gamma\right)
\end{aligned} \tag{16}$$

$$\text{on the line}: \frac{\mathrm{d}z}{\mathrm{d}t} = \tilde{c}_t|_3 \tag{17}$$

$$
\begin{aligned}
&-\nu\frac{R}{e}\frac{\rho_f|_4}{\rho_t}\frac{\left(\frac{c_F|_4}{c_t}\right)^2}{1-\left(\frac{c_F|_4}{\tilde{c}_t|_4}\right)^2}\left(\frac{\mathrm{d}V}{\mathrm{d}t}\right)_4\\
&+\nu\frac{R}{e}\frac{1}{\rho_t}\frac{1}{c_t}\frac{\tilde{c}_t|_4}{c_t}\frac{\left(\frac{c_F|_4}{\tilde{c}_t|_4}\right)^2}{1-\left(\frac{c_F|_3}{\tilde{c}_t|_3}\right)^2}\left(\frac{\mathrm{d}P}{\mathrm{d}t}\right)_4\\
&+\left[1+2\nu^2\frac{R}{e}\frac{\rho_f|_4}{\rho_t}\frac{\left(\frac{c_F|_4}{c_t}\right)^2}{1-\left(\frac{c_F|_4}{\tilde{c}_t|_4}\right)^2}\right]\left(\frac{\mathrm{d}u_z}{\mathrm{d}t}\right)_4\\
&+\frac{1}{\rho_t c_t}\frac{\tilde{c}_t|_4}{c_t}\left(\frac{\mathrm{d}\sigma_z}{\mathrm{d}t}\right)_4\\
&=\left[1+2\nu^2\frac{R}{e}\frac{\rho_f|_4}{\rho_t}\frac{\left(\frac{c_F|_4}{c_t}\right)^2}{1-\left(\frac{c_F|_4}{\tilde{c}_t|_4}\right)^2}\right]\left(\frac{\rho_f|_4 A_f}{\rho_t A_t}\frac{2}{\rho_f|_4 R}\tau_0+g\sin\gamma\right)\\
&+\nu\frac{R}{e}\frac{\rho_f|_4}{\rho_t}\frac{\left(\frac{c_F|_4}{c_t}\right)^2}{1-\left(\frac{c_F|_4}{\tilde{c}_t|_4}\right)^2}\left(\frac{2}{\rho_f|_4 R}\tau_0+g\sin\gamma\right)
\end{aligned}
\tag{18}
$$

$$
\text{on the line}: \frac{\mathrm{d}z}{\mathrm{d}t}=-\tilde{c}_t|_4 \tag{19}
$$

The entities that define the characteristic curves, called modified celerities in the fluid and in the pipe, are also obtained by applying the MOC method:

$$
\tilde{c}_F=\frac{1}{\sqrt{2}}\left\{\left\{c_F^2+c_t^2-\left[-4c_F^2c_t^2+\left(c_F^2+c_t^2+\frac{2c_F^2Rv^2\rho_f}{e\rho_t}\right)^2\right]^{\frac{1}{2}}+\frac{2c_F^2Rv^2\rho_f}{e\rho_t}\right\}^{\frac{1}{2}}\right\} \tag{20}
$$

$$
\tilde{c}_t=\frac{1}{\sqrt{2}}\left\{\left\{c_F^2+c_t^2+\left[-4c_F^2c_t^2+\left(c_F^2+c_t^2+\frac{2c_F^2Rv^2\rho_f}{e\rho_t}\right)^2\right]^{\frac{1}{2}}+\frac{2c_F^2Rv^2\rho_f}{e\rho_t}\right\}^{\frac{1}{2}}\right\} \tag{21}
$$

It is important to emphasize that, based on the assumptions made, this MOC transformation is carried out considering the coefficients as constant, and the celerities were

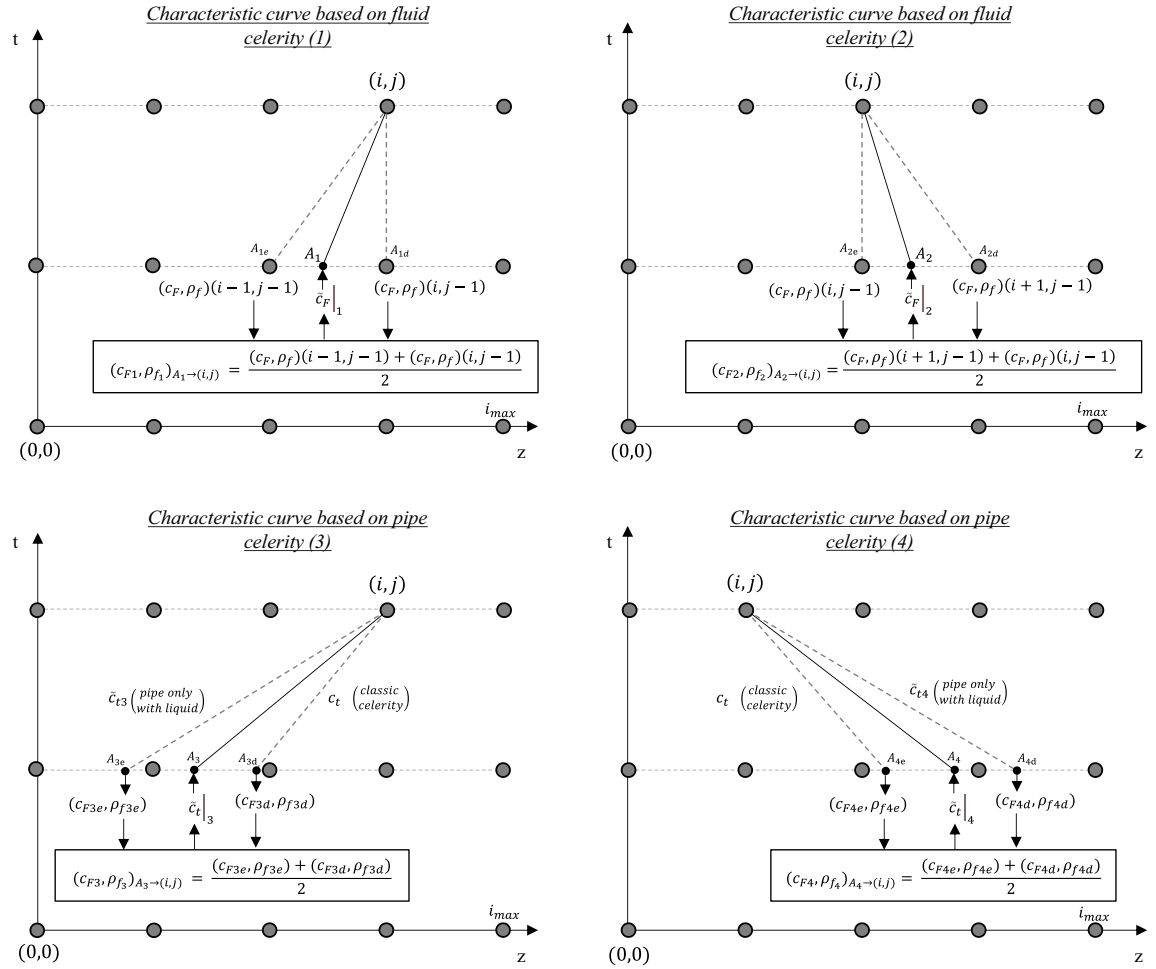

Fig. 2 Mesh, calculation of the celerities and definition of the characteristic curves of fluid and pipe for a given point (*i,j*). *Source*: Author

approximated with equal modules, and also constants, both for the fluid and for the pipe, establishing straight characteristic lines. However, for a two-phase fluid, it is known that the magnitude of the celerities varies according to the flow conditions, and the characteristic lines start to represent curved paths (variables) in the space–time domain. For the numerical solution, to incorporate the variable behavior of the properties, the coefficients of each compatibility equation will be treated as variables, being updated according to the flow condition, and the characteristic lines updated based on average values of the related properties, for each calculation step. That is, why the compatibility equations and characteristic lines presented in Eqs. (12)–(18), are adopting indices (with i varying from 1 to 4) for the differentials of interest $\left(\left(\frac{\mathrm{d}V}{\mathrm{d}t}\right)_i; \left(\frac{\mathrm{d}P}{\mathrm{d}t}\right)_i; \left(\frac{\mathrm{d}\dot{u}_z}{\mathrm{d}t}\right)_i; \left(\frac{\mathrm{d}\sigma_z}{\mathrm{d}t}\right)_i\right)$ and for the variable average properties $(\rho_f\big|_i; c_F\big|_i; \tilde{c}_F\big|_i; \tilde{c}_t\big|_i)$, according to each compatibility equation and characteristic line. The definition for how to obtain the average values of the properties, to be updated in each calculation step, is detailed in the numerical model explanation.

3 Numerical model

Initially, a numerical mesh is established for the solution through integration over the characteristic curves defined in the space–time domain, as shown in Fig. 2, with the number of time steps defined as input and the number of distance steps defined according to the condition of Courant ($\Delta z = \tilde{c}_F \Delta t$). A given point ($i$, j) is also shown, where i indicates the position of the point in the direction of the pipe dimension (z), and j is the position in the time dimension (t). Considering that same point, the characteristic curves (1 and 2) for the fluid and (3 and 4) for the pipe are defined, these curves being used so that the known values in the points of the previous step (A_1, A_2, A_3, A_4) can be obtained through linear interpolations. The valve is at $i = i_{\max}$ and the reservoir at $i = 0$.

For the solution of compatibility Eqs. (12)–(18) in the defined space–time domain, the equations are numerically integrated. In this way, a system of equations is produced that is solved to obtain the values of interest at the point (i,j): $(V, P, \dot{u}_z, \sigma_z)_{(i,j)}$. After solving this system, the void fraction $\alpha_{(i,j)}$ is calculated at the point, according to the isothermal expansion equation, as previously defined in Eq. (9):

$$\alpha_{(i,j)} = \alpha_0 \frac{p_0}{p_{(i,j)}} \tag{22}$$

It is important to highlight that the coefficients on the left side of the equations vary according to $\rho_f(\alpha)$ and $c_F(P,\alpha)$, and the parcels on the right side vary according to $\rho_f(\alpha)$, $c_F(P,\alpha)$, V and $\dot{u}_z$. For this reason, the referred coefficients and parcels are recalculated at each time step, taking the values of the variables of interest known in the previous step, so that they are then considered constant during the time integration of the current step. However, in order to obtain the values in the previous step, they must be captured according to each of the four characteristic curves, with directions that need to be defined based on: $\tilde{c}_F\big|_1, -\tilde{c}_F\big|_2, \tilde{c}_F\big|_3 - \tilde{c}_F\big|_4$. For these directions to be obtained, they are calculated based on estimated celerities taking an average within intervals selected in the previous step, intervals which are defined in different ways, depending on whether the curve comes from the celerity in the fluid or from the celerity in the pipe. For the curves arising from the celerity in the fluid (curves 1 and 2), the calculations of $\rho_f(\alpha)$ and $c_F(P,\alpha)$, so that the calculation of $\tilde{c}_F\big|_1$ and $\tilde{c}_F\big|_2$ (with the characteristic directions associated), are carried out as shown in Fig. 2. In this same figure, the procedure for the curves arising from the velocity in the pipe can also be observed (curves 3 and 4). It is then possible to solve the system.

It is noteworthy that the distance Δz between the points in the z direction is defined according to the Courant condition $\Delta z = \tilde{c}_F \Delta t$, considering only the celerity in the pure liquid, which is greater than in the two-phase fluid. Thus, the number of elements N in the pipe is calculated based on the chosen Δt, and the Δt is chosen so that at least 16 elements are obtained, a number considered reasonably capable of producing good results, based on the results presented by [6]. When considering a two-phase fluid, as the celerity is lower in this type of fluid, it is known that in the characteristic curves of the fluid (curves 1 and 2) the points and will always fall between the previous nodes: $(i-1, j-1)$ and $(i, j-1)$, $(i+1, j-1)$ and $(i, j-1)$, respectively. On the other hand, as for the pipe curves (curves 3 and 4), the celerities are significantly higher, the points and shall fall away from the immediately previous region, but the average celerity shall be between the celerity of the pipe completely filled with liquid ($\tilde{c}_t$) and the pipe without liquid (c_t), and those are used to limit the region where the calculations are performed for the curves 3 and 4, as also presented in Fig. 2.

It is observed in Fig. 2 that the characteristic curves intersect the previous step in intermediate spaces, between the points where the values are actually known. To obtain the values at the exact crossing point, a linear interpolation is performed in time (when there is intersection of the characteristic curves with the extremities) and in space (when there is intersection of the curves with intermediate spaces of the previous step).

In addition, the friction term τ_0 is calculated as follows (with "cur" ranging from 1 to 4, depending on the characteristic curve):

$$\tau_0 = \rho_f \frac{f V_{\text{rel}} \left| V_{\text{rel}} \right|}{8} \approx \rho_{f_{\text{cur}}} \frac{f V_{\text{rel}_{A_{\text{cur}}}} \left| V_{\text{rel}_{A_{\text{cur}}}} \right|}{8} \tag{23}$$

Thus, the solution is carried out for all intermediate nodes, following the described method, with further first-order finite difference integration.

3.1 Initial conditions

The initial conditions refer to the steady state before the hydraulic transient. The pipe is assumed to be in a steady state with constant flow. When defining the initial conditions, the values of the variables of interest along the pipe are established for the time $t=0$, that is, $P(z,0)$, $V(z,0)$, $\sigma_z(z,0)$ and $\dot{u}_z(z,0)$. The initial values are:

$$P(z,0) = P_{\text{reservoir}} - \left(\frac{f V_{\text{rel}} \left| V_{\text{rel}} \right|}{4gR} + \sin\gamma \right) \rho_l g z \tag{24}$$

$$V(z,0) = \text{constant} \tag{25}$$

$$\sigma_z(z,0) = \sigma_{z\,\text{value}} + \left(\frac{\rho_l f V_{rel} \left| V_{rel} \right|}{8e\left(1 + \frac{e}{2R}\right)} + \rho_t g \sin\gamma \right) (L - z) \tag{26}$$

$$\dot{u}_z(z,0) = 0 \tag{27}$$

To define the initial conditions, as there are no pressure peaks, and the void fraction is assumed to be very small, the density of the fluid is approximated by that of the liquid $\rho_f \approx \rho_l$, and the variables are calculated at all initial points ($t=0$). After this step, the calculated pressure at each point is used to calculate the void fraction $\alpha(z,0)$ at all initial points:

$$\alpha(z,0) = \frac{\alpha_0 p_0}{p(z,0)} \tag{28}$$

3.1.1 Boundary conditions

At the points located at the ends (reservoir and valve), only two characteristic curves are available. In this way, only two equations are available for the variables of interest to be obtained. Thus, the boundary conditions to be considered for these points are presented, so that all the variables of interest can be obtained at the extremities.

The reservoir is considered infinite, with constant pressure during the transient. This condition means that at the entrance of the pipe, the pressure is equal to that of the reservoir, whatever the time. Furthermore, it is considered that the piping is rigidly fixed to the reservoir, and both do not move.

$$P(0,t) = P_{\text{reservoir}} \tag{29}$$

$$\dot{u}_z(0,t) = 0 \tag{30}$$

The outlet valve is modeled as being rigidly fixed, with axial movement restriction, or being able to move axially. Furthermore, the closing time of the valve can be instantaneous, or it can vary depending on the condition to be simulated. The relations considered to satisfy the possibilities at the outlet valve are described in Table 1, where Cd is the valve discharge coefficient, defined by Eq. (30).

$$Cd = \left[1 - \left(\frac{t}{t_c} \right)^m \right] \tag{31}$$

4 Results and discussion

Four main verifications were made to evaluate the answers provided by the model developed in this paper. In general, the following analyses were carried out:

1. Suitability for single-phase flow: The results produced by the model presented in this paper were compared with the results available in the literature, considering a single-phase flow. This way, the goal was to verify (considering a case of flow simpler than two-phase and with more abundant results in the literature) whether the model structure and the information flow of the numerical model are working properly;

Table 1 Boundary conditions ate the outlet valve. *Source*: Author

Instantaneous closure and fixed valve		Instantaneous closure and free valve		Closure with variable time
$V(L,t) = 0$	(32)	$V(L,t) = \dot{u}_z(L,t)$	(34)	Equations (32) and (34) are replaced by:
$\dot{u}_z(L,t) = 0$	(33)	$A_f \Delta P = A_t \Delta\sigma_z$	(35)	$\Delta P = P_{\text{outlet}} + K_v \rho_f \frac{V_{\text{rel}} \left| V_{\text{rel}} \right|}{2}$ where $K_v = \frac{1}{Cd^2} - 1$

Table 2 Simulation data for comparison with single-phase fluid. *Source*: Author

Data	Value	Description
L	20.0	Pipe length [m]
t_{max}	0.1	Maximum time [s]
t_{points}	300	Number of simulation points in time
P_D	0.0	Initial pressure at the valve [m]
σ_{ZD}	0.0	Initial axial stress at the valve [Pa]
V_0	1.0	Initial fluid speed [m/s]
U_0	0.0	Initial pipe wall speed [m/s]
ρ_l	1000.0	Density of the liquid phase [kg/m^3]
ρ_t	7900	Density of the pipe [kg/m^3]
ν	0.3	Pipe Poisson coefficient
E	210*10^9	Pipe elasticity modulus [Pa]
K_l	2.1*10^9	Liquid phase bulk modulus [Pa]
f	0.02	Friction factor
R	0.399	Pipe internal radius [m]
e	0.008	Pipe wall thickness [m]
g	9.81	Gravity acceleration [m/s^2]
val_{cond}	free	Valve condition
α_0	0.0	Initial void fraction
P_{out}	2,026,500	Ambient pressure [Pa]
γ	0	Pipe angle
N	58	Number of pipe sub-elements (according to Courant condition)

2. Qualitative verification of behavior with two-phase flow: Two-phase flow was gradually introduced, and it was verified whether the qualitative behavior of the results produced was in accordance with what is physically expected;
3. Comparative verification with experimental data: Finally, a comparison of experimental results was carried out with the results produced by the model developed in this paper, thus obtaining a quantitative confirmation of the proper functioning of the model.
4. After these three steps of results assessments, the complete output chart of one simulation is presented for the reader to see the FSI behavior and also to be able to be sure that the FSI is properly captured by the model simulation.

In the next sub-chapters, the four main points presented herein will be detailed.

4.1 Suitability for single-phase flow

Initially, a direct comparison was made with the model produced by de Almeida [5] and with the exact solution of Tijsseling [4] for single-phase fluid. For that, the numerical model developed was used, considering the void fraction equal to zero, with input data according to Table 2 and producing results as shown in Fig. 3. The number of nodes in the mesh (mesh size) is characterized by the symbol "N," which was defined to be a number considerably higher than

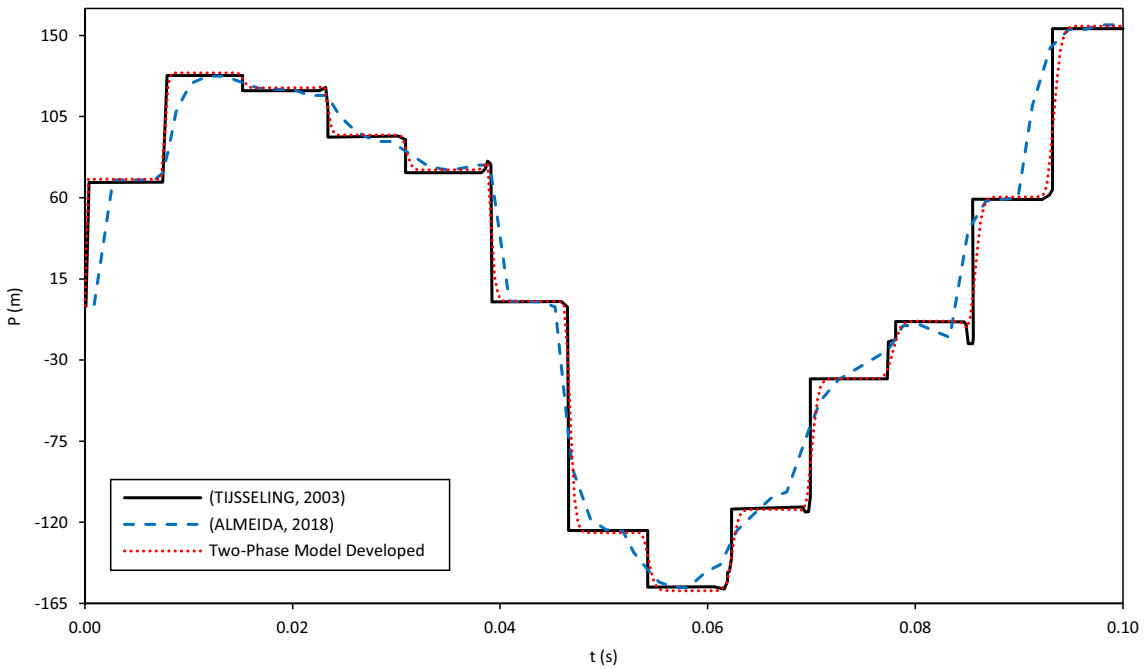

Fig. 3 Comparative single-phase result (valve instant closure)—Pressure × Time. *Source*: Author

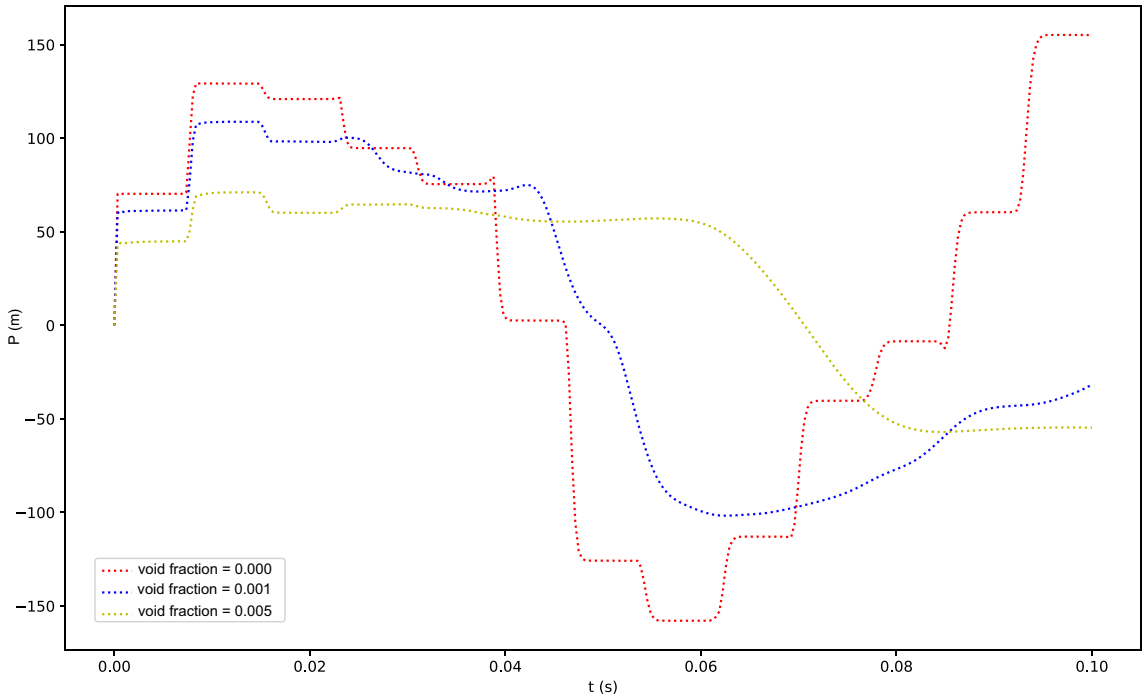

Fig. 4 Simulations results with increasing void fraction—Pressure × Time. *Source*: Author

eight, number assessed to produce good results for this simulation using MOC, after evaluating the results presented in Ref. [6].

After analyzing the results presented in Fig. 3, where it was considered instantaneous closure of the outlet valve, with the end free to move, it is possible to verify that the model manages to generate results even closer to the exact solution produced by Tijsseling [4], in comparison with the numeric results produced by de Almeida [5]. The results were even better than those of the model produced by de Almeida [5], possibly due to the fact that in the present paper, a new numerical model was fully developed in Python language, using a fully matrix data structure. This data structure is different from the array structure adopted in the model developed in the "C" language by de Almeida [5]. Furthermore, the model developed in this paper included the packages available in the Python environment for defining functions and calculating systems of equations, which can help to produce better results. It is also noteworthy that, when rewriting a new code, any possible existing and unchecked errors in the code may have been intrinsically corrected.

4.2 Qualitative verification of behavior with two-phase flow

From this point on, the behavior of the model is verified when a homogeneous two-phase fluid is incrementally

Table 3 Simulation data for comparison with experimental results. *Source*: Author

Data	Value	Description
L	30.6	Pipe length [m]
t_{max}	2.0	Maximum time [s]
t_{points}	800	Number of simulation points in time
P_D	12.5	Initial pressure at the valve [m]
σ_{ZD}	0	Initial axial stress at the valve [Pa]
V_0	2.94	Initial fluid speed [m/s]
U_0	0	Initial pipe wall speed [m/s]
ρ_l	1000	Density of the liquid phase [kg/m^3]
ρ_g	1	Density mass of the gaseous phase [kg/m^3]
ρ_t	7900	Density mass of the pipe [kg/m^3]
ν	0.3	Pipe Poisson coefficient
E	2.46*10^9	Pipe elasticity modulus [Pa]
K_l	2.1*10^9	Liquid bulk modulus [Pa]
f	0.0195	Friction factor
R	0.0127	Pipe internal radius [m]
e	0.00635	Pipe wall thickness [m]
g	9.81	Gravity acceleration [m/s^2]
val$_{cond}$	Fixed	Valve condition
α_0	0.0053	Initial void fraction
P_{out}	0.00001	Ambient pressure [Pa]
γ	0	Pipe angle
N	23	Number of pipe sub-elements (according to Courant condition)

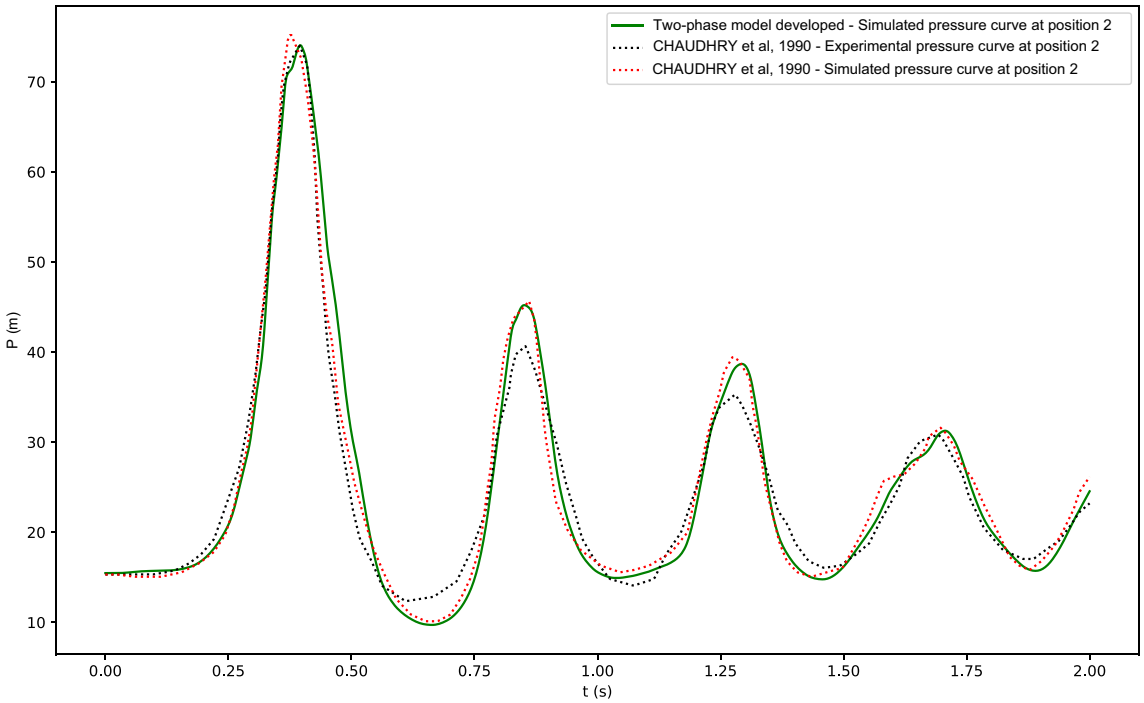

Fig. 5 Chart with comparison between simulation and experimental results—Pressure × Time. *Source*: Author

introduced. The same input data used for the validation of the single-phase fluid (Fig. 3) were considered, but with the addition of small increments of the initial void fraction ($\alpha_o = 0.001$ e $\alpha_o = 0.005$), so that it is possible to verify if the modification of the results occurs according to what is expected. In Fig. 4, the behavior of the curve can be seen as the void fraction increases.

Analyzing the result, it can be seen that the amplitude of the peaks is reduced with the increase in the void fraction and that the frequencies of the pulses also tend to be reduced, confirming the expected physical behavior, due to the reduction of the celerity in the fluid when compared with the single-phase fluid formed only by the liquid phase.

Table 4 Two-phase model main result—Pressure × Time. *Source*: Author

Item	Parameter	Result
Peak 1	P_{max} [m]	74.07
	t [s]	0.40
Peak 2	P_{max} [m]	45.21
	t [s]	0.85
Peak 3	P_{max} [m]	38.69
	t [s]	1.29
Peak 4	P_{max} [m]	31.27
	t [s]	1.71
Average frequency [Hz]		2.29

This result ensures that the model continues to be able to capture the behavior of the fluid, as demonstrated for the single-phase fluid, even with the introduction of the two-phase fluid.

4.3 Comparative verification with experimental data

In order to ensure the capability of the model to produce good results, the experiment carried out at the Georgia Institute of Technology [8] was considered, in which the behavior of a homogeneous two-phase fluid was analyzed when subjected to quick closure of the outlet valve. The input data considered for the developed model are presented in Table 3.

The comparative chart is shown in Fig. 5 (which refers to measurement "position 2" in the indicated experiment, meaning 9.5 m away from the outlet valve, on the z-axis), and the main simulation results are presented in Table 4. It is noteworthy that the thickness of the pipe used in the simulation goes a little beyond the condition of a thin-walled pipe, but it was still adopted so that it is identical to the acrylic pipe used in the experiment (according to data kindly shared by the Georgia Institute of Technology), and even carrying a possible deviation linked to this approximation, Fig. 5 shows that the results produced are quite consistent with experiment and simulation performed and presented by Chaudry et al. [8].

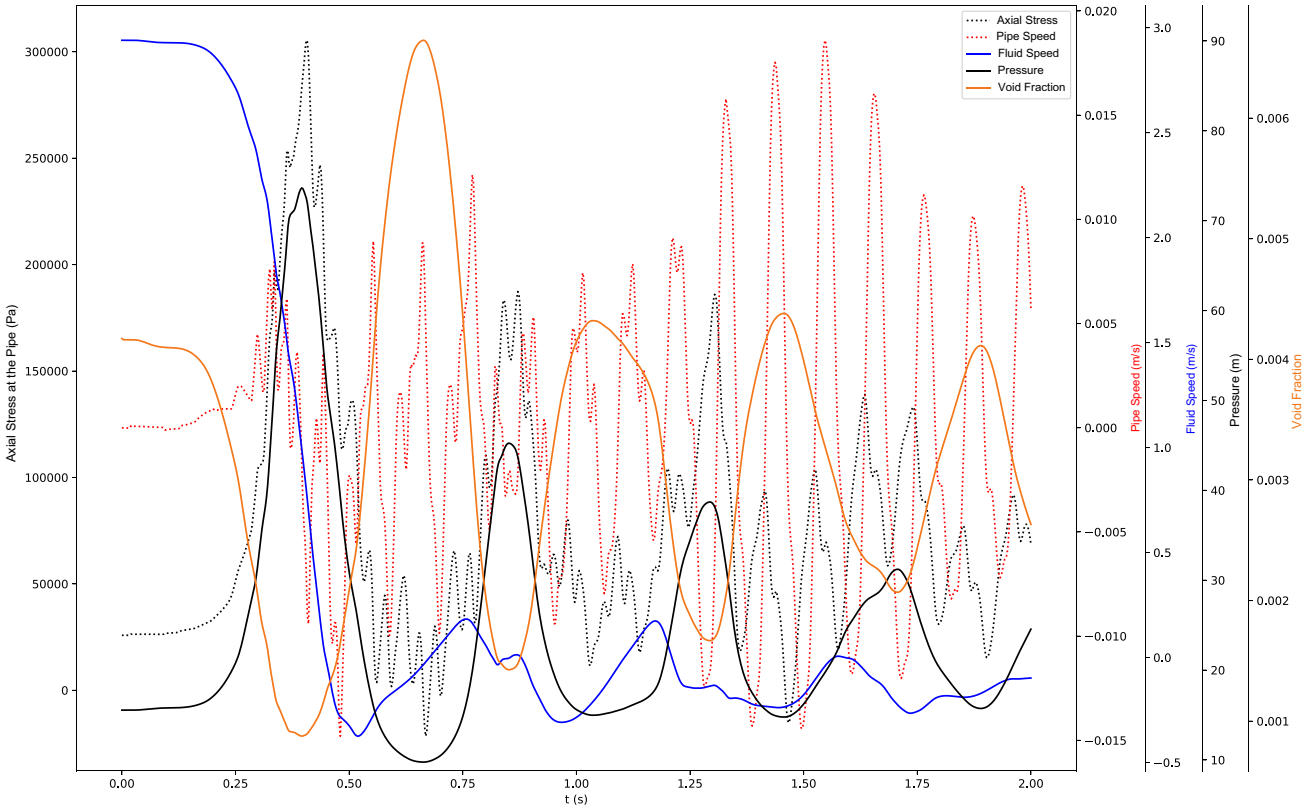

Fig. 6 Chart with complete two-phase model simulation result at the experimental region. *Source*: Author

4.4 Complete results output with FSI

Finally, as shown in Fig. 6, it can be verified that the results of the model developed actually encompass the FSI, leading this model to produce more comprehensive and complete results. Furthermore, it can be assessed for instance that the first pressure peak of the developed model was more adherent to the experimental results (as shown in Fig. 5) probably due to the consideration of the FSI because, as it is shown in Fig. 6, when the first pressure peak occurs, there is a local small reduction in the pipe axial stress, relaxation that normally leads to pressure reduction and that might be the physical behavior responsible for the better fitting of the pressure peak to the experiment.

5 Conclusion

A unidimensional model was developed and presented to capture the hydraulic transients in homogeneous two-phase flow with low void fraction, considering the fluid–structure interaction. The solution by the method of characteristics was adopted, and a methodology was presented for the mathematical and numerical treatment of variable celerity and density for this kind of fluid. The model, in general, was quite adherent to the experimental and analytical results, mainly in relation to the first pressure peak, which is one of the main focuses of the transient analyses. For future works and studies, it is suggested that more degrees of freedom are included in the analysis [6] and that other methods of solving the equations can be verified, different from the method of characteristics, such as those of finite differences including the convective terms proposed by Oloruntoba and Kara [3].

Acknowledgements The authors thank for the Brazilian Navy support and for the data kindly shared by Eindhoven University of Technology (Netherlands) and Georgia Institute of Technology (USA).

Authors contribution Each author contributed to the research presented in this manuscript, approved the contents now presented and agreed to the compliance with ethical standards.

Funding This research did not receive any specific grant from funding agencies in the public, commercial or not-for-profit sectors.

Availability of data and materials The manuscript has no associated data in a data repository.

Declarations

Conflict of interest The authors also declare that they have no competing financial interests or personal relationships that could have influenced this research.

Consent to publish Both authors consent to the manuscript's publication in the JBSMSE, should the article be accepted by the Editor upon completion of the refereeing process.

Ethical approval The manuscript is original and has not been submitted for publication elsewhere (partially or in full). Also, the manuscript has not been submitted to more than one publication for simultaneous consideration.

References

1. Bonin CC (1960) Water-hammer damage to Oigawa power station. J Eng Power 82:111–116. https://doi.org/10.1115/1.3672721
2. van Duyne DA, Merilo M (1996) Water hammer handbook for nuclear plant engineers and operators. Electric Power Research Institute (EPRI), TR-106438
3. Oloruntoba O, Kara F (2017) Simplified transient two-phase model for pipe flow
4. Tijsseling AS (2003) Exact solution of linear hyperbolic four-equation system in axial liquid-pipe vibration. J Fluids Struct 18:179–196
5. de Almeida RSP (2018) Modelo numérico para cálculo do Transitório Hidráulico e Interação Fluido-Estrutura em sistemas de transporte de fluidos. Dissertação de Mestrado, Universidade de São Paulo (USP)
6. Tijsseling AS (1993) Fluid-structure interaction in case of water hammer with cavitation. Ph.D. Thesis
7. Chaudhry MH (2014) Applied hydraulic transients, 3rd edn. Springer, New York
8. Chaudry MH, Bhallamudi SM, Martin CS, Naghash M (1990) Analysis of transient pressures in bubbly, homogeneous, gas-liquid mixtures. J Fluids Eng 112:225–231
9. Fernandes LS (2017) Medição do Campo de Velocidade do Líquido no Escoamento Bifásico, Intermitente, em Duto Horizontal, Utilizando Velocimetria Estereoscópica. Tese de Doutorado, PUC-Rio
10. Thorley ARD (2004) Fluid transients in pipeline systems: a guide to the control and suppression of fluid transients in liquids in closed conduits, 2nd edn. Professional Engineering Publishing Limited, London
11. Záruba J (1993) Water hammer in pipe-line systems. Elsevier, Amsterdam